

## Brownian vortexes

Bo Sun,<sup>1</sup> Jiayi Lin,<sup>2</sup> Ellis Darby,<sup>2</sup> Alexander Y. Grosberg,<sup>1</sup> and David G. Grier<sup>1</sup>

<sup>1</sup>*Department of Physics and Center for Soft Matter Research, New York University, New York, NY 10003*

<sup>2</sup>*NEST+m, 111 Columbia Street, New York, NY 10002*

A particle diffusing around a point of stable mechanical equilibrium in a static but non-conservative force field enters into a steady state characterized by circulation in the probability flux. Circulation in such a Brownian vortex is not simply a deterministic response to the solenoidal component of the force, but rather reflects an interplay between force-driven probability currents and diffusion. As an example of this previously unrecognized class of stochastic heat engines, we consider a colloidal sphere stably trapped in a conventional optical tweezer. Rather than coming into thermodynamic equilibrium with the surrounding heat bath, the particle's Brownian fluctuations are biased into a toroidal roll. We demonstrate both theoretically and experimentally that the circulation in this practical realization of the Brownian vortex can undergo flux reversal.

Stochastic heat engines such as thermal ratchets and Brownian motors use non-conservative forces to eke a flux of energy or probability out of otherwise random thermal fluctuations [1]. Unlike deterministic machines, these systems would not operate at all without the motivating influence of thermal noise. Although a great many mechanisms have been proposed for implementing stochastic heat engines, virtually all rely on time dependence in the force field to rectify fluctuations. Here, we demonstrate that time-independent force fields also can create stochastic heat engines, provided the force has a non-vanishing solenoidal component. The resulting steady-state probability currents feature circulating rolls, which inspire us to name such systems Brownian vortexes. We demonstrate both theoretically and experimentally that Brownian vortexes arise naturally in the motions of colloidal spheres localized in optical traps, and that the probability flux can reverse direction with continuous changes in such control parameters as the laser power or temperature.

Our discussion focuses on the behavior of a single particle immersed in a viscous medium that also acts as a thermodynamic heat bath. The particle is acted upon by a static force field,

$$\mathbf{F}(\mathbf{r}) = -\nabla U + \nabla \times \mathbf{A}, \quad (1)$$

that is factored uniquely into a conservative irrotational component described by the scalar potential  $U(\mathbf{r})$  and a non-conservative solenoidal component derived from the vector potential  $\mathbf{A}(\mathbf{r})$ . In the absence of thermal forcing, the particle is assumed to come to a stable mechanical equilibrium at a point  $\mathbf{r}_0$  for which  $\mathbf{F}(\mathbf{r}_0) = 0$ .

Were it not for thermal forces, the particle would remain motionless at  $\mathbf{r}_0$ . Thermal fluctuations enable the particle to explore the force field with a probability density  $\rho(\mathbf{r})$  that does not depend on time in steady state. The local probability flux,

$$\mathbf{j}(\mathbf{r}) = \mu \rho(\mathbf{r}) \mathbf{F}(\mathbf{r}) - \mu k_B T \nabla \rho(\mathbf{r}), \quad (2)$$

reflects both the particle's response to the force field through its mobility,  $\mu$ , and also its diffusivity at temper-

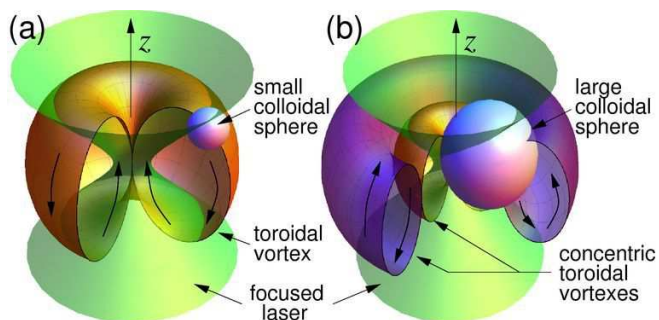


FIG. 1: (Color online) Schematic representation of a colloidal sphere undergoing toroidal circulation in an optical tweezer. (a) The Rayleigh limit,  $a < \lambda$ . (b) The Mie and ray-optics limits,  $a > \lambda$ .

ature  $T$ . Because the probability is conserved,  $\nabla \cdot \mathbf{j} = 0$ , and the flux either vanishes in equilibrium ( $\nabla \times \mathbf{A} = 0$ ) or else forms closed loops in steady state ( $\nabla \times \mathbf{A} \neq 0$ ). Circulation around these loops is measured by

$$\nabla \times \mathbf{j} = \mu \rho \boldsymbol{\omega} + \mu \nabla \rho \times \mathbf{F}, \quad (3)$$

where  $\boldsymbol{\omega}(\mathbf{r}) = -\nabla^2 \mathbf{A}$  is the vorticity in  $\mathbf{F}(\mathbf{r})$  [2]. Vortexes can form in  $\mathbf{j}(\mathbf{r})$  even if  $\mathbf{F}(\mathbf{r})$  does not have closed loops because the diffusive flux represented by the second term in Eq. (3) provides the return flow.

Both the magnitude and the direction of  $\boldsymbol{\omega}(\mathbf{r})$  can vary with position. The rate and direction of the particle's circulation therefore depend on the domain over which the particle can diffuse at temperature  $T$ . Changing the temperature changes this range and therefore can reverse the sense of the overall circulation. The possibility of temperature-dependent flux reversal distinguishes Brownian vortex circulation from the more familiar interplay of advection and diffusion in such systems as the electric current flowing through a battery-powered circuit.

As a concrete example of the Brownian vortex phenomenon, we consider the motions of a colloidal sphere in an optical tweezer [3], a single-beam optical gradient force trap that consists of a strongly focused beam of

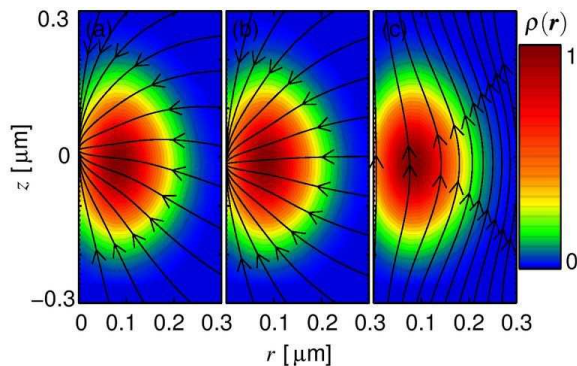


FIG. 2: (Color online) (a) Streamlines of the optical force  $\mathbf{F}(\mathbf{r})$  in the  $(r, z)$  plane exerted on a  $0.4 \mu\text{m}$  radius polystyrene sphere in water by a  $532 \text{ nm}$  optical tweezer focused with a numerical aperture 1.4 lens. (b) Streamlines of the irrotational component of the force,  $-\nabla U$ . (c) Streamlines of the solenoidal component of the force,  $\nabla \times \mathbf{A}$ . Shading indicates the relative probability density  $\rho(\mathbf{r})$  at  $T = 21^\circ\text{C}$  and a laser power of  $0.3 \text{ W}$ .

light [3]. Recent particle-tracking measurements [4] overturned the conventional understanding that a trapped particle comes to thermodynamic equilibrium within an optical tweezer, revealing instead a circulating steady state indicated schematically in Fig. 1(a). The original explanation for these observations [4] relied on an idealized model for the optical forces acting on a sphere in which intensity gradients drew the sphere to the focal point with a Hookean force and radiation pressure displaced the particle downstream with a force proportional to the local intensity. This model predicts the appearance of a single toroidal vortex in  $\rho(\mathbf{r})$  directed downstream along the optical axis and returning upstream at larger displacements.

Light scattering by colloidal particles is more complicated than suggested by this model, particularly for particles such as those studied in Ref. [4] that are larger than the wavelength of light [5, 6]. Figure 2(a) shows streamlines of the force field computed with Lorenz-Mie theory [7] for a micrometer-diameter polystyrene sphere in water trapped within an optical tweezer. The trap is formed from a laser beam with a vacuum wavelength of  $\lambda = 532 \text{ nm}$  propagating in the  $\hat{z}$  direction and brought to a focus by an ideal lens with numerical aperture 1.4. Streamlines are projected into the  $(r, z)$  plane in cylindrical coordinates,  $\mathbf{r} = (r, \phi, z)$ . Figures 2(b) and (c) show the irrotational and solenoidal components of the force field, respectively, and were obtained through the Helmholtz-Hodge decomposition [2] of  $\mathbf{F}(\mathbf{r})$ .

The particle's thermally driven trajectory  $\mathbf{r}_p(t)$  through this force field was computed with a Brownian dynamics simulation of the Langevin equation

$$\dot{\mathbf{r}}_p = \mu \mathbf{F}(\mathbf{r}_p) + \mu \mathbf{f}(t), \quad (4)$$

where  $\mu = (6\pi\eta a)^{-1}$  is the Stokes mobility for a sphere of

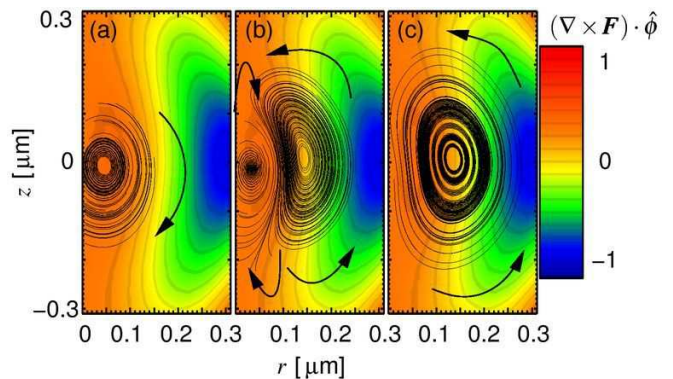


FIG. 3: (Color online) Computed streamlines of a  $0.4 \mu\text{m}$  radius polystyrene sphere diffusing in the optical force field of Fig. 2. (a) Forward circulation at  $P = 0.7 \text{ W}$ . (b) Concentric counter-rotating vortices at  $P = 0.5 \text{ W}$ . (c) Complete flux reversal at  $P = 0.3 \text{ W}$ .

radius  $a$  moving through a fluid of viscosity  $\eta$ , and where the stochastic force due to thermal fluctuations satisfies  $\langle \mathbf{f}(t) \rangle = 0$  and  $\langle \mathbf{f}(t) \cdot \mathbf{f}(t') \rangle = 2\mu^{-1}k_B T \delta(t - t')$ . The probability distribution and flux then are computed with nonparametric density estimators [8] as

$$\rho(\mathbf{r}) = \frac{1}{(2\pi\sigma)^{3/2}} \left\langle \exp\left(-\frac{|\mathbf{r} - \mathbf{r}_p(t)|^2}{2\sigma^2}\right) \right\rangle \quad \text{and} \quad (5)$$

$$\mathbf{j}(\mathbf{r}) = \frac{1}{(2\pi\sigma)^{3/2}} \left\langle \mathbf{r}_p(t) \exp\left(-\frac{|\mathbf{r} - \mathbf{r}_p(t)|^2}{2\sigma^2}\right) \right\rangle, \quad (6)$$

where  $\sigma$  is chosen to minimize the variance in  $\rho(\mathbf{r})$  without unnecessary blurring. This approach lends itself to direct comparison between simulation and experimental measurements of colloidal trajectories.

Shading in Fig. 2 represents the probability density  $\rho(\mathbf{r})$  at  $T = 21^\circ\text{C}$  for an optical tweezer powered by  $P = 0.3 \text{ W}$ . Neither,  $\mathbf{F}(\mathbf{r})$  nor its solenoidal component display loops in this range. Nevertheless, the streamlines of  $\mathbf{j}(\mathbf{r})$ , plotted in Fig. 3 show loops in the  $(r, z)$  plane consistent with the appearance of a toroidal vortex centered on the optical axis. It should be emphasized that the observed circulation is apparent only in a very long trajectory or in an ensemble average of shorter trajectories; at short times, the particle's motion resembles a random walk in a harmonic well, its toroidal bias too subtle to be perceived.

Figure 3(a) shows streamlines at a comparatively large laser power,  $P = 0.7 \text{ W}$ , for which the particle is well localized near the optical axis. Under these conditions, the particle circulates in a single toroidal vortex, much as was predicted in Ref. [4] and portrayed in Fig. 1(a). The local circulation rate,  $[\nabla \times \mathbf{j}(\mathbf{r})] \cdot \hat{\phi}$ , is uniformly positive.

Reducing the laser power does not change the structure of the force field, but reduces its overall magnitude. This is equivalent, therefore, to increasing the effective temperature. Doing so increases the range over which the

particle can wander and enables it to populate a second, concentric counter-rotating vortex, as plotted in Fig. 3(b) for  $P = 0.5$  W, and indicated schematically in Fig. 1(b).

At still lower laser power (or higher temperature), the outer vortex supplants the inner vortex, and the probability current circulates once again in a single toroidal roll, but with its direction reversed. This flux reversal is demonstrated in Fig. 3(c) for  $P = 0.3$  W.

The origin of the flux reversal in Brownian vortex circulation can be seen in the vorticity of the force field in Fig. 3. Although the solenoidal component of the optical force,  $\nabla \times \mathbf{A}$ , is directed uniformly upward,  $\nabla \times \mathbf{F}$  changes direction with distance from the optical axis. So long as the particle's probability density is concentrated in regions where  $\boldsymbol{\omega}(\mathbf{r}) \cdot \hat{\boldsymbol{\phi}}$  is positive, as is the case in Fig. 3(a), the overall circulation of the probability flux also is positive. When the particle wanders into regions of negative vorticity, it circulates in the retrograde direction, as shown in Fig. 3(b). In both cases, the non-conservative part of the optical force field redistributes  $\rho(\mathbf{r})$  downstream of the beam's focal point and diffusion provides the return current. The single-roll structure reasserts itself in the flux-reversed state when gradients in  $\rho(\mathbf{r})$  become large enough for diffusion to outstrip advection along the optical axis.

We also observed flux reversal in Brownian vortex circulation through experimental observations of colloidal spheres trapped in optical tweezers. Our system consists of 1.5 nm diameter colloidal silica spheres (Bangs Labs, Lot SS04N/5252) dispersed in a 50  $\mu\text{m}$  thick layer of water that is hermetically sealed between a clean glass slide and a No. 1.5 cover slip. The sample is mounted on the stage of an inverted light microscope (Nikon TE 2000U) where it is observed with a 100 $\times$  numerical aperture 1.4 oil immersion objective lens (Nikon Plan Apo). The same objective lens is used to focus four holographic optical tweezers [9, 10, 11, 12] arranged at the corner of a square with 30  $\mu\text{m}$  sides near the midplane of the sample. These traps are powered by a single laser (Coherent Verdi 5W) operating at a vacuum wavelength of  $\lambda = 532$  nm that is imprinted with a computer-generated hologram [11] by a liquid-crystal spatial light modulator (Hamamatsu X7665-16) before being projected into the sample. The trap array is designed so that two of the traps have nearly the same intensity, the third is slightly brighter, and the fourth brighter still. This enables us to seek out intensity-dependent differences in simultaneously acquired data sets, and thus to avoid possible systematic effects due to vibrations or other instrumental fluctuations.

The trapped spheres' three-dimensional motions are measured with nanometer resolution through quantitative analysis [13] of images obtained with holographic video microscopy [14, 15]. Holographic images are obtained by illuminating the sample with the collimated beam from a HeNe laser (Uniphase 10 mW) operating at

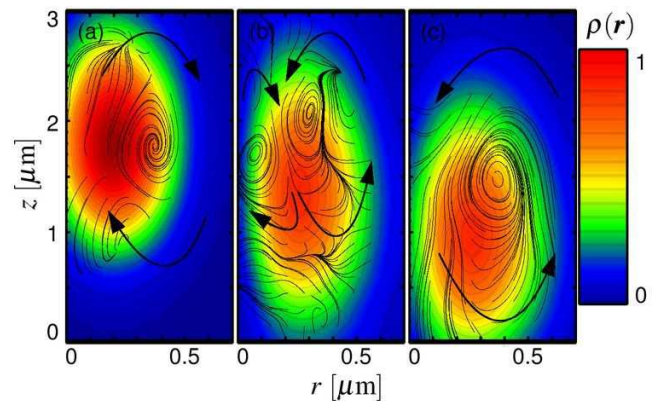


FIG. 4: (Color online) Streamlines of the measured circulation of colloidal silica spheres trapped in optical tweezers. (a)  $k_{\perp} = 6.56$  pN/ $\mu\text{m}$ : Single roll circulating in the positive sense. (b)  $k_{\perp} = 2.43$  pN/ $\mu\text{m}$ : Concentric counter-rotating rolls. (c)  $k_{\perp} = 2.27$  pN/ $\mu\text{m}$ : Flux reversal. Single retrograde roll. Background images show the particles' measured probability densities.

632.8 nm. Light scattered by the particles interferes with the unscattered portion of the beam in the microscope's focal plane to create an in-line hologram that is magnified and recorded by a video camera (NEC TI-324AII) at 30 frames per second. Radiation pressure due to the nW/ $\mu\text{m}^2$  intensity of the imaging beam is negligible compared with thermal forces and forces due to the optical trap and so does not affect the particles' trajectories.

Both fields of each interlaced holographic video frame were analyzed with Lorenz-Mie light scattering theory [5, 13] to measure each sphere's three-dimensional position  $\mathbf{r}(t)$ , with 3 nm in-plane resolution and 10 nm axial resolution [13]. A total of thirty two-minute-long trajectories were acquired at constant laser power for the four particles. At the end of each acquisition period, the trapped particles were moved automatically out of the field of view to acquire background holograms and to confirm the system's stability. Each particle's trajectories were analyzed with Eqs. (5) and (6) to visualize the mean circulation and the results combined into maps of the mean circulation for each trap. In all, more than 100,000 holograms were analyzed for each trap.

Figure 4 shows streamlines of the trajectories for three of the four particles, the fourth serving as a control for Fig. 4(c). These results confirm not only the presence of toroidal circulation in the particles' motions, but also the appearance of flux reversal as a function of trap strength. Each trap-particle combination is characterized by its apparent [4] in-plane stiffness,  $k_{\perp}$ , which is obtained from statistical analysis of the particle's measured in-plane fluctuations [11], stiffer traps generally corresponding to higher laser power and lower effective temperature. The traps' apparent axial stiffness is a factor of 5 smaller than their lateral stiffness because axial intensity gradients are

correspondingly weaker [4, 16].

The stiffest trap, shown in Fig. 4(a), concentrates its particle's probability density  $\rho(\mathbf{r})$  closest to the optical axis and displays a single roll circulating in the positive sense. The weaker trap in Fig. 4(b) allows the trapped particle to wander further afield, where it enters into concentric counter-rotating rolls, similar to the simulated results in Fig. 3(b). The weakest traps, one of which is represented in Fig. 4(c), both display a single retrograde roll in  $\mathbf{j}(\mathbf{r})$ , and thus demonstrate complete flux reversal.

The probability distribution is centered lower in the weaker traps because of gravity acting on the silica spheres, whose  $1.9 \text{ g/cm}^3$  density exceeds that of the surrounding water. This additional conservative force does not directly contribute to the particles' circulation but does affect what region of the optical force field the particle occupies for a given laser power. Undoubtedly, this influenced the trend in Fig. 4, but does not change our interpretation of the phenomenon as flux reversal in a Brownian vortex.

Instrumental fluctuations cannot account for our observations because all four measurements were performed simultaneously in a static array of optical traps derived from the same laser beam. The particles are sufficiently separated from each other and from the walls of their container that hydrodynamic coupling also is unlikely to have influenced their motion [17]. Rather, Brownian vortex circulation, including power-dependent flux reversal, appears to be an inherent aspect of the statistics of colloidal spheres in optical tweezers.

In this study, we have introduced the Brownian vortex as a distinct class of noise-driven machines. Unlike stochastic heat engines driven by time-dependent forces, Brownian vortices are driven out of equilibrium by the solenoidal component of a static force field. Because one-dimensional force fields have no solenoidal component, the Brownian vortex has no one-dimensional manifestation. Not any static force field, furthermore, can support a Brownian vortex. For example, a force field lacking a stable equilibrium point cannot establish the requisite probability-conserving steady-state. Still other force fields establish circulating steady states without thermal noise. An example of this is provided by the ring-like optical trap known as an optical vortex [18] that exerts torques on trapped objects [19] through its helical wavefront structure [20]. These are deterministic machines rather than stochastic heat engines, and so are not Brownian vortices.

Although the illustrative simulations and experiments presented here focus on colloidal circulation in optical tweezers, the Brownian vortex is a more general phenomenon. Seeking its signature in such contexts as biological networks and financial systems, as well as in new mechanical models, should provide opportunities for future research. Further work also is required to elucidate Brownian vortices' thermodynamic properties, particu-

larly the considerations that determine their thermodynamic efficiency.

We acknowledge fruitful conversations with Yohai Roichman. This work was supported by the MRSEC program of the NSF under grant number DMR-0820341. B.S. acknowledges support from the Kessler Family Foundation.

- 
- [1] P. Reimann, R. Bartussek, R. Haussler, and P. Hänggi, *Phys. Lett. A* **215**, 26 (1996); H. Linke, *Appl. Phys. A* **75**, 167 (2002); R. D. Astumian and P. Hänggi, *Physics Today* **55**, 33 (2002); P. Reimann, *Phys. Rep.* **361**, 57 (2002); P. Reimann and P. Hänggi, *Appl. Phys. A* **75**, 169 (2002).
  - [2] L. Morino, *Comp. Mech.* **1**, 65 (1986).
  - [3] A. Ashkin, J. M. Dziedzic, J. E. Bjorkholm, and S. Chu, *Opt. Lett.* **11**, 288 (1986).
  - [4] Y. Roichman, B. Sun, A. Stolarski, and D. G. Grier, *Phys. Rev. Lett.* **101**, 128301 (2008).
  - [5] C. F. Bohren and D. R. Huffman, *Absorption and Scattering of Light by Small Particles* (Wiley Interscience, New York, 1983).
  - [6] A. Ashkin, *Biophys. J.* **61**, 569 (1992).
  - [7] B. Sun, Y. Roichman, and D. G. Grier, *Opt. Express* **16**, 15765 (2008).
  - [8] B. W. Sliverman, *Density Estimation for Statistics and Data Analysis* (Chapman & Hall, New York, 1992).
  - [9] E. R. Dufresne and D. G. Grier, *Rev. Sci. Instrum.* **69**, 1974 (1998).
  - [10] D. G. Grier, *Nature* **424**, 810 (2003).
  - [11] M. Polin, K. Ladavac, S.-H. Lee, Y. Roichman, and D. G. Grier, *Opt. Express* **13**, 5831 (2005).
  - [12] Y. Roichman, A. S. Waldron, E. Gardel, and D. G. Grier, *Appl. Opt.* **45**, 3425 (2006).
  - [13] S.-H. Lee, Y. Roichman, G.-R. Yi, S.-H. Kim, S.-M. Yang, A. van Blaaderen, P. van Oostrum, and D. G. Grier, *Opt. Express* **15**, 18275 (2007).
  - [14] J. Sheng, E. Malkiel, and J. Katz, *Appl. Opt.* **45**, 3893 (2006).
  - [15] S.-H. Lee and D. G. Grier, *Opt. Express* **15**, 1505 (2007).
  - [16] K. C. Vermeulen, G. J. L. Wuite, G. J. M. Stienen, and C. F. Schmidt, *Appl. Opt.* **45**, 1812 (2006).
  - [17] J. C. Crocker, *J. Chem. Phys.* **106**, 2837 (1997); E. R. Dufresne, T. M. Squires, M. P. Brenner, and D. G. Grier, *Phys. Rev. Lett.* **85**, 3317 (2000); E. R. Dufresne, D. Altman, and D. G. Grier, *Europhys. Lett.* **53**, 264 (2001); M. Polin, D. G. Grier, and S. R. Quake, *Phys. Rev. Lett.* **96**, 088101 (2006).
  - [18] H. He, N. R. Heckenberg, and H. Rubinsztein-Dunlop, *J. Mod. Opt.* **42**, 217 (1995); N. B. Simpson, L. Allen, and M. J. Padgett, *J. Mod. Opt.* **43**, 2485 (1996); K. T. Gahagan and G. A. Swartzlander, *Opt. Lett.* **21**, 827 (1996).
  - [19] H. He, M. E. J. Friese, N. R. Heckenberg, and H. Rubinsztein-Dunlop, *Phys. Rev. Lett.* **75**, 826 (1995).
  - [20] L. Allen, M. W. Beijersbergen, R. J. C. Spreeuw, and J. P. Woerdman, *Phys. Rev. A* **45**, 8185 (1992); Y. Roichman, B. Sun, Y. Roichman, J. Amato-Grill, and D. G. Grier, *Phys. Rev. Lett.* **100**, 013602 (2008).